

# Geometric and Nonequilibrium Criticality in Run-and-Tumble Particles with Competing Motility and Attraction

Abir Bhowmick,<sup>\*</sup> Sayantan Mitra,<sup>†</sup> and P. K. Mohanty<sup>‡</sup>

Department of Physical Sciences, Indian Institute of Science Education and Research Kolkata, Mohanpur, 741246 India.

Self-propulsion in run-and-tumble particles (RTPs) generates effective attractive interactions that can drive motility-induced phase separation (MIPS), a phenomenon absent in their passive counterparts. In this work, we show that at high motility, introducing explicit attractive interactions among RTPs can suppress MIPS, leading to a homogeneous phase, and subsequently induce a re-emergence of phase separation at stronger attraction — thus realizing a re-entrant phase transition. We characterize this transition by examining the percolation properties of dense clusters, which serve as geometric signatures of phase separation. Along the resulting critical line, we observe continuously varying critical exponents, while some of the associated scaling functions remain invariant and coincide with those of equilibrium lattice gas models undergoing interacting percolation, which is Ising-percolation universality. These findings reveal that the MIPS transition in interacting RTPs exhibits Ising-like super universality, bridging nonequilibrium active matter with classical critical behavior.

## I. INTRODUCTION

Active matter is a special class of nonequilibrium systems where the constituents self-propel by consuming energy from the environment [1]. A vast range of systems composed of motile or self-propelled particles fall within this class. Some examples include flocks of birds [2], fish schools [3], actin filaments [4] and microtubules [5] in the context of the study of locomotion and colloidal systems [6–9]. Two of the simplest and most widely studied models of active particle dynamics are the *run-and-tumble particles* (RTPs) [10, 11] and the *active Brownian particles* (ABPs) [12]. In the case of ABPs, the direction of motion changes smoothly via rotational diffusion at each time step, whereas in RTPs, there is a period of persistent motion in a given direction (the principal direction) called “run”, followed by a sudden change of direction called “tumble”. This simplified model is studied extensively in the context of the motion of *E. Coli* [13].

Among the many fascinating characteristics shown by active particle systems, such as non-equilibrium steady-states [12, 14–17], clustering [18, 19], ratchet effects [20]; the most intriguing one that draws the attention of many researchers is the motility-induced phase separation (MIPS) [21–25] where the particles, even in the absence of any attractive interaction, form high-density clusters well separated from a low-density region. In particular, when the speed of active particles decreases with increasing local density, a uniformly mixed suspension becomes unstable. This instability gives rise to phase separation, resulting in the coexistence of a dilute, motile gas phase and a dense, less motile liquid phase. This sustained phase-separated state (PS state), arising without any attractive interactions, is one of the most fascinating phenomena observed in active matter systems. While

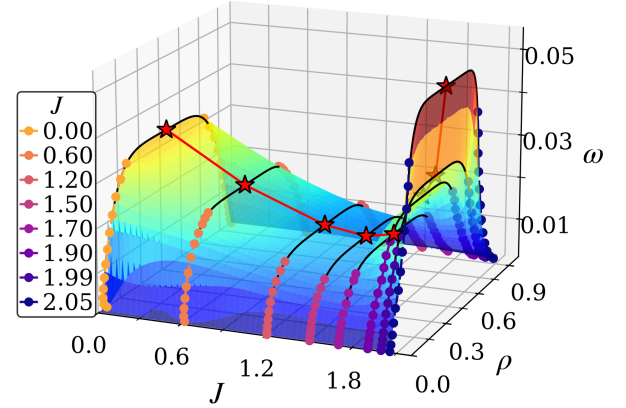


FIG. 1. (Color online) The 3D phase diagram of RTP model in  $J$ - $\rho$ - $\omega$  phase space. Interpolation of the co-existence lines in the  $\rho$ - $\omega$  plane for different  $J$  values leads to a surface that separates the mixed phase from the PS state. The zero-gradient condition forms a line (the critical line) on this surface. The critical points ( $J_c, \rho_c, \omega_c$ ) obtained from simulations align well with this critical line.

most of the studies are based on numerical simulations, there are a few theoretical studies that employ hydrodynamic analysis [1, 26, 27], some use agent-based modeling [28, 29], and also there are lattice-based approaches [18, 19, 30–33]. In one dimension (1D), even though hydrodynamic analysis supports the existence of MIPS [34] a recent lattice-based study cast doubt on it [33]. However, in two dimensions (2D), numerous on-lattice [35–37] and off-lattice [38–41] models exhibit MIPS transition. Persistent motion of active particles is essential for phase separation, but it alone does not guarantee it. A recent study [42] demonstrates that passive particles undergoing phase separation due to inter-particle attraction  $J$ , as in a lattice gas model, require significantly stronger attraction to phase separate once motility is introduced. In fact, no MIPS was observed when the attraction was absent ( $J = 0$ ). A later on-lattice study of RTPs with zero

<sup>\*</sup> ab23rs019@iiserkol.ac.in

<sup>†</sup> sayantan.pdf@iiserkol.ac.in

<sup>‡</sup> pkmohanty@iiserkol.ac.in

attraction ( $J = 0$ ) [43], showed that translational diffusion, which allows particles to move beyond their primary propulsion direction, plays a crucial role in enabling the MIPS transition. By examining the relation between percolation phenomena and phase separation, the authors suggested that the MIPS transition may belong to the Ising super universality class, characterized by continuously varying critical exponents alongside some scaling functions similar to those of the equilibrium lattice gas phase separation. This interpretation aligns with several other studies [35, 42, 44, 45] proposing that MIPS transitions fall within the 2D IUC.

It is well known that active particles generate an effective pairwise attraction due to their persistent motion [14, 22, 23] but it is quite counterintuitive that additional attraction reduces the effect! However, a recent study [46] illustrates analytically that effective short-range repulsion can emerge among active Brownian particles (ABPs) interacting via attractive potentials. In this article, we study the effect of attractive interaction  $J$  on a system of hard-core RTPs on a lattice and investigate its impact on the MIPS transition. Each RTP has an internal sense of direction pointing along one of the four nearest neighbors (square lattice). In the “run” event, particles can move to any of the nearest neighbors, but with a relatively higher rate to a neighbor along its internal orientation. Whereas in a “tumble” event, the particle flips its internal direction to any of the other three. The inverse tumbling rate plays the role of motility. We find that in the high motility regime (low tumbling rate), additional attractive interaction indeed destroys the phase separated (PS) state, as with increased attraction the system undergoes a phase transition from PS state to mixed phase, but soon it regains the PS state as one keeps increasing the interaction strength. We find that the critical exponents of this MIPS transition vary continuously along the critical line in the  $\omega$ - $J$  plane. This transition, however, belongs to the Ising super universality class in the sense that, though the critical exponents vary continuously along the critical line some of the scaling functions turn out to be identical to those of the usual equilibrium PS transition in the 2D lattice gas model.

The article is organized as follows: in section II we briefly describe the model and the limiting cases of the parameters involved in it in detail. In section III, we discuss the choice of order parameters and the corresponding difficulty associated with it, for the systematic study of the geometric transition property (percolation) and underlying phase separation transition. Then in section IV, we present the numerical details associated with the study of the percolation transitions and MIPS transition. In subsequent section V, we analyze the role of density for systems having no particle-hole symmetry (like 2D lattice gas/Ising models), in determining the critical parameters and the associated static exponents. Next in section VI, we show that the phase separation transition of the interacting RTPs belong to the  $Z_2$  super universality class. In the end, in section VII, we conclude the

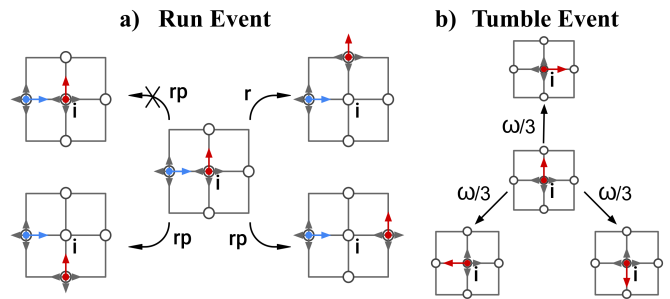


FIG. 2. (Color online) Dynamics of IRTP model: One RTP  $k$  (chosen out of  $N$ ), with site index  $\mathbf{i}$  and internal orientation  $\theta_k = \frac{\pi}{2}$  (pointing up) can (a) run, or (b) tumble with indicated rates. Here  $r = \min(1, e^{-\Delta E})$  is the Metropolis rate wrt Eq. (1), the parameter  $0 \leq p < 1$  generates translational diffusion, and  $\omega > 0$  is a constant tumble rate.

important findings.

## II. THE MODEL

We consider  $N$  RTPs on a square lattice  $\mathcal{L}$  of  $L^2$  sites labeled by  $\mathbf{i} \equiv (x, y)$ , with  $x, y = 1, 2, \dots, L$  and use periodic boundary conditions in both  $x$  and  $y$  directions. Each site  $\mathbf{i}$  has an occupation number  $n_{\mathbf{i}} = \{0, 1\}$  that represents if the site is vacant or filled up. Due to the hardcore (excluded volume) interaction, each site can be occupied by at most one RTP, imposing a constraint on the total number of particles:  $\sum_{\mathbf{i}} n_{\mathbf{i}} = N$ . Each RTP, labeled as  $k = 1, 2, \dots, N$  has an intrinsic orientation  $\theta_k \in \{0, \frac{\pi}{2}, \pi, \frac{3\pi}{2}\}$  that determines the direction of dominant movement to the nearest neighbor in  $\theta_k$  direction, i.e., from the site  $\mathbf{i}$  to the direction  $\mathbf{i} + \boldsymbol{\delta}_k$ , where  $\boldsymbol{\delta}_k = (\cos(\theta_k), \sin(\theta_k))$ . Note, that  $\mathbf{i} + \boldsymbol{\delta}_q$  with  $\boldsymbol{\delta}_q = (\cos(q\frac{\pi}{2}), \sin(q\frac{\pi}{2}))$ ;  $q = 0, 1, 2, 3$ , are the four nearest neighbors of a site  $\mathbf{i} \in \mathcal{L}$ .

Besides the hardcore interaction, the RTPs experience a nearest-neighbor attraction, described by an energy function

$$E = -J \sum_{\mathbf{i} \in \mathcal{L}} \sum_{q=0}^3 n_{\mathbf{i}} n_{\mathbf{i} + \boldsymbol{\delta}_q} \quad (1)$$

where  $J > 0$ . Due to the presence of attractive interaction among the RTPs, we refer to this model as the interacting RTPs (IRTP) model. Note that the internal orientation of RTPs do not contribute to energy; they only dictate their direction of motion. During a “run” event, an RTP at the site  $\mathbf{i}$  moves to one of its neighbors with a Metropolis rate  $r = \min\{1, e^{-\Delta E}\}$ , where  $\Delta E$  is the difference in energy between final and initial configurations. The selection of neighbors is however asymmetric, with a ratio of  $1 : 3p$  between the internal orientation and the remaining three spatial directions. This parameter  $0 \leq p \leq 1$  accommodates the translational diffusion of RTPs. In addition to “run”, an RTP can “tumble”

with rate  $\omega$  and change its internal orientation to any of the other three lattice directions, chosen randomly. A schematic picture of the run and tumble events is described in Fig. 2.

We intend to study the phase separation transition of this IRTP model using Monte Carlo simulations, which will be discussed in the subsequent sections. But before that, let us look at some interesting limits.

*$p = 1$  case:* For  $p = 1$ , RTPs choose any of the four directions with equal probability. Then, the internal orientation is no more special, and tumbling loses its meaning. The dynamics then become identical to that of the conserved lattice gas (CLG) model in 2D with the temperature set at  $T = 1$ . Thus like CLG, one would expect the IRTP system to exhibit an equilibrium PS transition at  $J = J_c^*$ ,  $\rho = 1/2$  belonging to the Ising universality class (IUC), characterized by the critical exponents  $\nu^I = 1$ ,  $\beta^I = 1/8$ ,  $\gamma^I = 7/4$  (superscript I is used to denote Ising system).

*$p = 0$  case:* For  $p = 0$  the IRTP model reduces to what has been studied earlier in [42]. In this case, particles can run only along their internal orientation with the Metropolis rate. In the  $\omega \rightarrow \infty$  limit, the internal orientation of particles changes too often between two consecutive run events; in effect the dynamics of the model reduce to that of the CLG model, leading to a PS transition at  $J = J_c^*$ . For any finite  $\omega$ , the PS transition occurs at a critical interaction  $J_c(\omega)$ , which is larger than  $J_c^*$ . This indicates that in the absence of any translational diffusion ( $p = 0$ ), increased motility ( $\omega^{-1}$ ) hinders cluster formation and the system requires stronger attraction among particles to phase separate.

*$J = 0$  case:* In the absence of any interaction, our model closely resembles the model studied recently in [43], with the only difference that tumbling of internal orientation  $\theta \rightarrow \theta + \pi$ , was absent there. Using a mapping between phase separation and percolation, the authors found a re-entrant MIPS transition in the  $\omega$ - $p$  plane: the system phase separates at intermediate  $p$  but remains mixed at both low and high  $p$ . These findings align well with the absence of MIPS at  $p = 0$ ,  $J = 0$  studied in Ref. [42] and the lack of transition at  $J = 0$ ,  $p = 1$ , corresponding to the 2D symmetric exclusion process.

The IRTP system we study has both translational diffusion and attractive interaction which serves as an essential foundation for capturing the interplay between MIPS transition and conventional phase separation. It has been suggested that the MIPS transition in RTPs belongs to the IUC [44]. Incorporating attraction among particles brings this model closer in spirit to many off-lattice active matter systems, where interparticle interactions play a key role in phase separation [41, 47, 48]. This framework also provides a natural bridge between MIPS and the phase separation behavior observed in 2D CLG models. Through our work, we focus on the geometric aspects of the IRTP system by studying the percolation transition of RTPs and utilize the known mapping between percolation and phase separation to ex-

tract the critical exponents associated with the underlying MIPS transition in the presence of attractive interactions.

### III. RELATION BETWEEN PHASE SEPARATION AND PERCOLATION TRANSITIONS

In the PS state, the density of the system is not homogeneous and the coarse-grained density profile breaks translational symmetry, which is observed as an emergent instability in hydrodynamic theory [21, 49]. In this phase, the system separates into coexisting high- and low-density regions with densities  $\rho_+$  (liquid) and  $\rho_-$  (gas) respectively, while the conserved particle density  $\rho = N/L^2$  is absent locally throughout the system. In the mixed phase, the mean local density of the system is expected to be equal to this density  $\rho$  with the system having a translationally invariant coarse-grained density profile.

In the case of 2D CLG model, where particles interact via the nearest neighbor attraction similar to that of Eq. (1), it is well known that the system exhibits a PS state when the interaction strength  $J$  is lowered below a threshold value  $J_c^* = 2(\ln(1 + \sqrt{2}))$ , called the Onsager value (in units  $k_B = 1$  and  $T = 1$ ) [50]. In this limit, the system co-exists in phases having two different densities  $\rho_+$  and  $\rho_-$ , forming a coexistence line in the  $\rho$ - $J$  plane with its maxima at  $(\rho_c, J_c^*)$ ; with  $\rho_c = 1/2$ . Above this critical point, the coexistence ceases to exist and a mixed phase appears. Even if one considers  $\langle \rho_+ \rangle - \langle \rho_- \rangle$  as the order parameter of the PS transition as it vanishes in the mixed phase, the difficulty lies in determining the exact value of the critical density where liquid and gas co-existence lines meet. This is because at  $\rho \simeq \rho_c$ , the curvature of the co-existence line is usually very low and the change in the properties of the system is not significant unless one changes the density appreciably. But the presence of the particle-hole symmetry (same as  $Z_2$ ) in CLG, dictates the critical density to be  $\rho_c = 1/2$  and hence it is not hard to determine the critical value of the other parameter  $J_c$  from numerical simulations. The absence of such symmetry in the PS transition and hence in the MIPS transition makes the determination of the critical point and respective critical exponents harder because one needs to tune two parameters ( $\rho_c$ ,  $J_c$ ) simultaneously now, instead of one. To overcome this challenge we follow the method in [44, 51], and without any loss of generality, we assume the critical density of PS transition to be  $\rho = \rho_c = 1/2$  throughout our study unless otherwise stated. Later we demonstrated that  $\rho_c$  is indeed very close to  $1/2$  and showed that the critical line and the static exponents are insensitive to the slight change of critical density around this expected value. This insensitivity of  $\rho_c$  has been indicated earlier in several studies [41, 43, 44, 51].

Another difficulty in the study of PS transition of active particles is the choice of the order parameter. When

the system is undergoing a PS transition, the onset of the transition can be understood from the density histogram, as it changes the one-peaked nature and forms a double-peaked profile. Also, the power spectrum of the density correlation of the system exhibits a power-law divergence in the zero momentum limit. While both these methods distinguish a PS state from a mixed one, they suffer from strong finite-size corrections. To determine the critical point accurately in active matter systems, Binder and co-workers in their subsequent studies [41, 51, 52] proposed a scheme called the sub-box method, that can be implemented on a rectangular lattice having an aspect ratio of 3:1. The scheme is to consider a  $6\ell \times 2\ell$  simulation box with  $N$  particles and place four  $\ell \times \ell$  square sub-boxes in each steady-state configuration of the system for efficient sampling of the density. Two of them, called dense boxes, are placed parallel to the simulation box positioned around the center of mass (COM) in  $x$ -direction [53], on top of each other along  $y$ -direction. The other two (dilute boxes) are placed at a distance  $3\ell$  from the COM in  $x$ -direction, efficiently measuring the dilute region while avoiding the interface between the two zones. Thus each configuration in the steady state is sampled through these four measurement boxes. Let  $N_{\pm}$  be the number of particles in one of each dense and dilute boxes selected at random and  $\Delta N_{\ell} = N_{+} - N_{-}$  be their difference. Then a suitable order parameter that characterizes the PS transition can be defined as

$$\tilde{\phi} = \frac{1}{\ell^2} \langle \Delta N_{\ell} \rangle = \langle \rho_{+} \rangle - \langle \rho_{-} \rangle \quad (2)$$

where  $\langle \cdot \rangle$  represents the steady-state averages and  $\rho_{\pm} = N_{\pm}/\ell^2$  are the densities of dense and dilute regions as sampled by the selected measurement sub-boxes in a PS state, formally known as the liquid and gas densities. Note that,  $\tilde{\phi}$  vanishes in the mixed phase where  $\langle \rho_{+} \rangle = \langle \rho_{-} \rangle$ .

In this sub-box method, although the simulation runs on an elongated box, the sub-boxes are  $\ell \times \ell$  squares, and the correlation length  $\xi$  does not suffer a directional asymmetry at least in a region far from criticality where  $\xi \ll 2\ell$ . However, the fact that the average particle density  $\langle \rho \rangle$ , of all four measurement boxes is different from the conserved input density  $\rho = \frac{N}{12\ell^2}$ , may generate an additional loss of precision due to non-conservation. Also reaching a larger  $\ell$  to trace the actual behavior of active particle systems is quite difficult. To overcome these difficulties another approach is considered in [42], where the aspect ratio was chosen to be 2 : 1 instead of 3 : 1, such that the system size is  $L_x = 2\ell$  and  $L_y = \ell$ . The order parameter they used, though respects the conserved particle density  $\rho$  but the implemented aspect ratio of 2 : 1 does not rule out additional sampling issues due to the prominent interface overlap. Since an accurate estimate of critical exponents is essential for determining the universality class of a continuous phase transition, we look into the geometric properties of the system from the perspective of percolation theory and try to exploit

its connection with the underlying PS transition following the recent work as in [43].

Usually in a PS state the high-density region is formed by a singly connected component whereas the low-density region has many disconnected clusters. Here a unique cluster is constructed, similar to those defined in the site-percolation problems [54], by connecting two particles if they are nearest neighbors of each other. Although during the evolution of the system, the large macro-cluster may break down, a single cluster is always energetically favorable. Thus a PS transition is always associated with a geometric percolation transition where the size of the largest cluster serves as the order parameter of the system. Note that any configuration of  $N$  particles on a lattice can be viewed as a collection of  $K$  clusters, indexed as  $k = 1, 2, \dots, K$ , each containing  $s_k$  number of particles so that  $\sum_{k=1}^K s_k = N$ . If  $s_{\max} = \max\{s_k\}$  is the size of the largest cluster, then one can consider  $\phi = s_{\max}/L^2$  as the order parameter of the system to characterize the geometric transition, similar to that used in site-percolation problems [54–57]. In the mixed phase, the cluster is typically as large as the finite correlation length  $\xi$  (for  $\xi \ll L$ ) of the system, which makes  $\phi \rightarrow 0$  in the thermodynamic limit  $L \rightarrow \infty$ . On the other hand, in the PS state as the clusters occupy a finite fraction of the particles thereby becoming comparable to system size and hence leading to  $\phi \neq 0$ .

Then the percolation order parameter  $\phi$  and susceptibility  $\chi$  are defined in a same manner as in ordinary percolation [54]

$$\phi = \frac{1}{L^2} \langle s_{\max} \rangle; \quad \chi = \frac{1}{L^2} (\langle s_{\max}^2 \rangle - \langle s_{\max} \rangle^2) \quad (3)$$

The associated critical exponents  $\nu$ ,  $\beta$ ,  $\gamma$ , related to the correlation length of the system, order parameter, and susceptibility as:  $\xi \sim |\varepsilon|^{-\nu}$ ,  $\phi \sim |\varepsilon|^{\beta}$ ,  $\chi \sim |\varepsilon|^{-\gamma}$  respectively, together determine the universality class of the system. In the context of equilibrium phase transitions, the site-percolation transition of CLG occurs exactly at the same critical interaction where PS transition occurs, but their critical exponents differ [58–61]. The static critical exponents of the PS transition of CLG in 2D are no different from that of the ferromagnetic transition:  $\nu^I = 1$ ,  $\beta^I = 1/8$ ,  $\gamma^I = 7/4$  (where the superscript I stands for Ising), and hence it can be said that the critical behavior belongs to the IUC or  $Z_2$  symmetry breaking. Since the percolation transition in CLG occurs at the same critical point, the correlation length remains the same and hence the associated correlation exponent  $\nu$  must remain the same in both transitions. It was argued by Stella and Vanderzande [62] that even though both the percolation and PS transition share the same critical point, the exponents of the geometric transition can not be expressed solely in terms of the Ising exponents. They conjectured that the fractal dimension of the percolating cluster at the critical point is not simply

$d_f = d - \beta^I/\nu^I = 15/8$ , rather it is

$$d_f = d - w \frac{\beta^I}{\nu^I}; \quad w = \frac{5}{12} \quad (4)$$

where the additional parameter  $w$  is determined from the connection of percolation with tri-critical  $q = 1$ -Potts model [62]. The robustness of this relation is verified in many other models in 2D [61]. Thus the exponents of percolation  $\{\nu, \beta, \gamma\}$  are related to that of the underlying phase transition exponents  $\{\nu^I, \beta^I, \gamma^I\}$  as

$$\nu = \nu^I, \quad \beta = \frac{5}{12}\beta^I, \quad \gamma = \frac{13}{12}\gamma^I \quad (5)$$

where  $\gamma$  is determined from the scaling relation  $2\beta + \gamma = d\nu$  [54, 63]. It is worth mentioning that percolation transition in CLG with exponents  $\nu = 1$ ,  $\beta = 5/96$ ,  $\gamma = 91/48$ , forms a different universality class called interacting percolation or  $Z_2$ -percolation ( $Z_2P$ ) universality [62].

Inspired by the observation that percolation properties efficiently capture the nature of the underlying PS transition and that their critical exponents are connected through simple scaling relations, we prefer to study the percolation properties of this IRTP system on a square lattice and try to infer about the critical exponents of the PS transition using Eq. (5). In a few cases, we will also verify the relations directly from the study of the PS transition with  $\phi$  (Eq. (2)) as the order parameter. The benefit of studying percolation transition is that we can consider a square geometry that evades ill effects of the slab geometry, if any. Moreover, cluster properties can be computed more efficiently in comparison to the determination of high and low densities  $\rho_{\pm}$  and corresponding density fluctuations.

#### IV. SIMULATIONS AND RESULTS

In the Monte-Carlo (MC) simulation of the IRTP model, a particle  $k$ , is chosen at random independently from the collection of  $N$  particles; say its position is  $\mathbf{i}$  and internal orientation is  $\theta_k$  (the unit vector along this direction is  $\delta_k = (\cos(\theta_k), \sin(\theta_k))$ ). The chosen particle can either decide to “tumble” with rate  $\omega$  to change this intrinsic orientation to any of the other three or “run” with rate  $r = \min\{1, e^{-\Delta E}\}$  to one of its nearest neighbors chosen as follows: site  $\mathbf{i} + \delta_k$  and other three neighbors in ratio  $1 : 3p$  distributed equally. Here,  $\Delta E$  is the change in energy of initial and final configurations, following Eq. (1). The detailed implementation of the dynamics is described in the Supplemental Material [64].

##### A. Percolation of interacting RTPs

We investigate the percolation transition of RTPs using MC simulations of the above model by varying the interaction strength  $J$ , while fixing the particle density

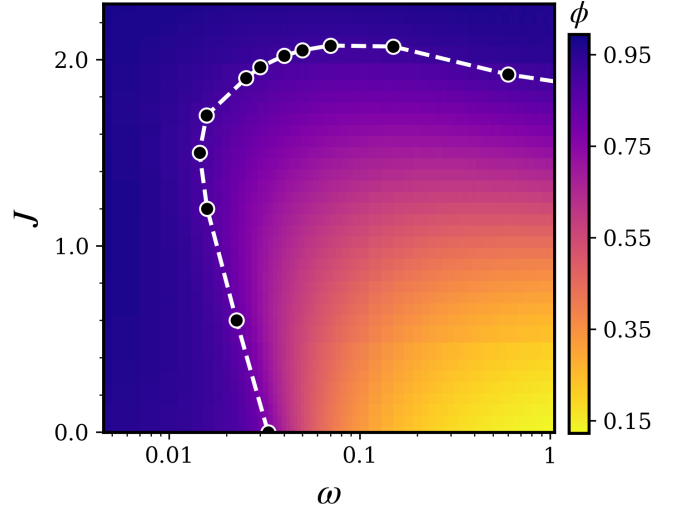


FIG. 3. (Color online) Density plot of the percolation order parameter  $\phi = \langle s_{\max} \rangle / L^2$  in the  $J$ - $\omega$  plane. The estimated critical points (circles) are joined by a line; this critical line separates the percolating phase from a non-percolating one and it coincides with the critical line of phase separation transition (see Fig. 7). The system size taken to produce the density plot is  $64 \times 64$  with particle density  $\rho = \frac{1}{2}$ .

at  $\rho = 1/2$  and the translational diffusion at  $p = 0.05$ . These values will be kept fixed throughout the study unless stated otherwise. To study the percolation transition we chose the order parameter as in Eq. (3), generally used to characterize geometric phase separation in percolation problems. A quantity of particular interest is the so-called Binder Cumulant  $B_L$ ,

$$B_L = 1 - \frac{\langle s_{\max}^4 \rangle}{3\langle s_{\max}^2 \rangle^2} \quad (6)$$

which is especially useful in the case of continuous phase transitions, because it takes a universal value at the critical point, independent of system size  $L$ . For the determination of critical point  $\omega_c$ , we then evaluate the Binder cumulant  $B_L$  as a function of  $\omega$  across different system sizes  $L$ ; their intersection point provides a good estimate of the critical value. For  $J_c = 0.6$ , this method yields  $\omega_c = 0.0225(2)$ , as shown in Fig. 4 (a). To calculate the critical exponents of the percolation transition, we employ the finite-size scaling (FSS) relations of  $B_L$ ,  $\phi$ , and  $\chi$ ,

$$B = f_B(\varepsilon L^{\frac{1}{\nu}}); \quad \phi = L^{-\frac{\beta}{\nu}} f_{\phi}(\varepsilon L^{\frac{1}{\nu}}); \quad \chi = L^{\frac{\gamma}{\nu}} f_{\chi}(\varepsilon L^{\frac{1}{\nu}}) \quad (7)$$

This suggests that  $B_L$ ,  $\phi L^{\beta/\nu}$  and  $\chi L^{-\gamma/\nu}$  must collapse onto a unique scaling function when one plots them against the quantity  $\varepsilon L^{1/\nu}$ . Since we know  $\varepsilon = \omega - \omega_c$ , one can use  $1/\nu$ ,  $\beta/\nu$  and  $\gamma/\nu$  as fitting parameters and hence can determine their value as the one which gives the best data collapse. Following this prescription we obtain the critical exponents  $\nu = 0.77(3)$ ,  $\beta = 0.041(3)$  and  $\gamma = 1.458(60)$ , corresponding to ( $\omega_c = 0.0225$ ,  $J_c = 0.6$ ).

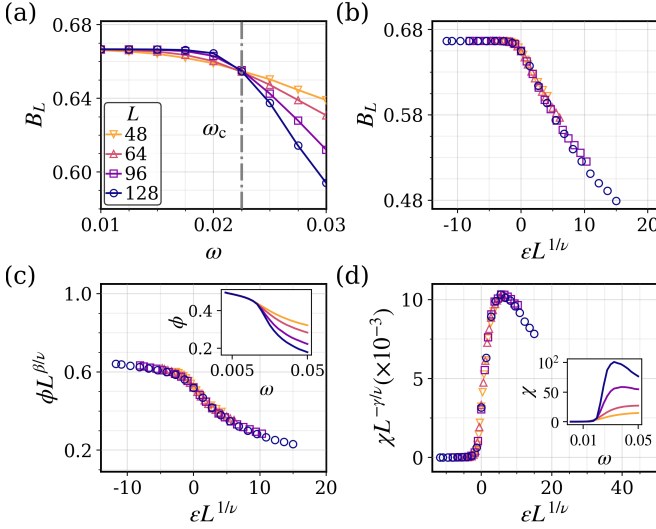


FIG. 4. (Color online) Finite-size scaling of Percolation transition in IRTP model at  $J_c = 0.6$ ,  $\rho_c = \rho = \frac{1}{2}$ . (a) Estimation of critical point  $\omega_c = 0.0225(2)$  from the crossing point of  $B_L$  vs  $\omega$  curve for different system sizes:  $L = 48, 64, 96, 128$ . (b), (c), and (d) provide scaling collapse of  $B_L$ ,  $\phi$ ,  $\chi$  according to Eq. 7, provide estimates of the critical exponents  $\nu = 0.77(3)$ ,  $\beta = 0.041(3)$  and  $\gamma = 1.458(60)$ .

$J_c$	$\omega_c$	$\nu$	$\beta$	$\gamma$
0.00(0)	0.0330(2)	0.84(1)	0.058(3)	1.564(20)
0.60(0)	0.0225(2)	0.77(3)	0.041(3)	1.458(60)
1.20(0)	0.0158(2)	0.72(2)	0.033(1)	1.374(40)
1.50(0)	0.0144(4)	0.76(3)	0.034(1)	1.452(60)
1.70(0)	0.0157(2)	0.78(3)	0.035(2)	1.490(60)
1.90(0)	0.0253(2)	0.91(2)	0.043(2)	1.734(40)
1.99(2)	0.0300(0)	0.92(2)	0.044(1)	1.752(40)
2.05(2)	0.0500(0)	0.95(2)	0.044(2)	1.812(40)
1.92(2)	0.6000(0)	1.05(3)	0.048(2)	2.044(60)
1.84(2)	2.0000(0)	1.04(3)	0.050(3)	1.980(60)
1.81(2)	3.0000(0)	1.04(2)	0.052(3)	1.976(40)

TABLE I. Critical points and corresponding static exponents of percolation transition of IRTP model at density  $\rho_c = 0.5$ .

This is shown in Fig. 4 (b),(c) and (d) respectively. In the insets of (c), and (d) we have shown the raw data.

A closer inspection of the phase plot in Fig. 3 reveals that for small values of  $J$  (approximately  $J < 1.9$ ) one can find the critical  $\omega_c$  by varying  $\omega$ , for a fixed  $J$ . For larger  $J$ , this would result in two critical points, as the transition appears to be re-entrant in nature. Then determination of critical parameters would influence each other, resulting in erroneous estimation. To overcome this, we consider changing  $J$  for a fixed  $\omega$ ; the scaling properties as in Eq. (7) remain the same, but one must consider  $\varepsilon = J - J_c$ . The critical points and the exponents  $\nu, \beta, \gamma$  determined from FSS analysis are listed in Table I. Details of the scaling collapse for all these studies are reported in the Supplemental Material [64].

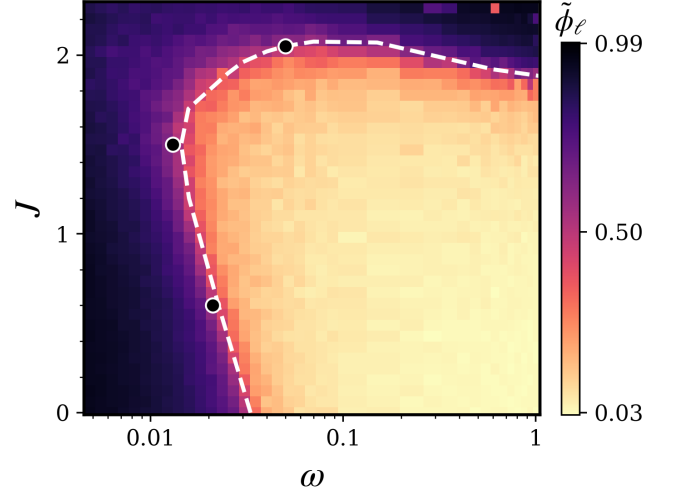


FIG. 5. (Color online) Density plot of order parameter  $\tilde{\phi}$  (Eq. (2)), for a  $6\ell \times 2\ell$  system to study PS transition with  $\ell = 36$ . Estimated critical points (circles) are shown along with the critical line of percolation transition obtained in Fig. 3. Within error limits they match well, suggesting that the percolation transition and PS transition occurs simultaneously and they share the same critical points along the critical line. Note that the conserved particle density taken for this case is  $\rho = \frac{1}{2}$ .

## B. MIPS transition of RTPs

Following several studies [60, 62] one can find that, the percolation transition in the 2D CLG model serves as a geometric signature of the underlying magnetic phase transition (PS transition). Notably, both the percolation and PS transition share the same critical temperature (or interaction), and the corresponding critical exponents are linked as outlined in Eq. (5). As established in previous studies [43] and further confirmed in a later section of this work, the percolation transition in RTPs belongs to the  $Z_2P$  super universality class, while the MIPS transition is believed to fall within the 2D Ising universality class (or  $Z_2$  universality)[44]. Since geometric and PS transition of RTPs are similar to that of the equilibrium CLG model, one can draw a correspondence between them, which allows one to reasonably propose that the percolation transition of RTPs and the underlying PS transition should also share the same critical point and an analogous relation between the respective critical exponents:

$$\nu^M = \nu, \quad \beta^M = \frac{12}{5}\beta, \quad \gamma^M = d\nu^M - 2\beta^M \quad (8)$$

where  $d$  is the spatial dimension and the superscript  $M$  denotes the exponents belong to MIPS transition. To verify Eq. (8), we would need the corresponding static exponents of MIPS transition and for that, we then employ the sub-box method [41] described earlier for the determination of critical point and those static exponents using order parameter  $\hat{\phi}$  as in Eq. (2). For the sake of

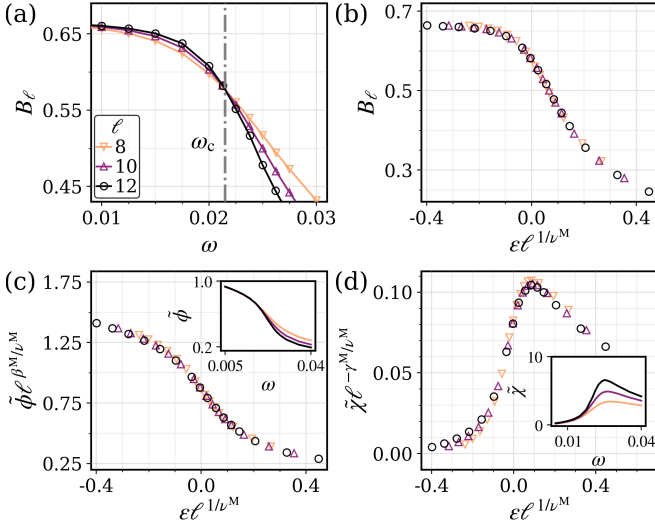


FIG. 6. (Color online) PS transition in IRTP model at  $J = 0.6$  and,  $\rho = 0.5$  (a) Estimate of the critical point from the crossing point of Binder cumulant  $B_\ell$  (Eq. (9)) vs  $\omega$  for different  $\ell = 8, 10, 12$ . Within error limits estimated critical point,  $\omega_c = 0.0215(2)$  matches with the same obtained from percolation transition. (b), (c), and (d) provide estimates of the critical exponents,  $\nu^M = 0.78(3)$ ,  $\beta^M = 0.12(3)$ ,  $\gamma^M = 1.32(8)$  from finite size scaling similar to Eq. (7).

comparison with the percolation study, here we define Binder cumulant of  $\tilde{\phi}$

$$B_\ell = 1 - \frac{\langle \Delta N_\ell^4 \rangle}{3 \langle \Delta N_\ell^2 \rangle^2} \quad (9)$$

to determine the critical point  $\omega_c$  at  $J_c = 0.6$ . From the cross of Binder cumulant  $B_\ell(\omega)$  calculated as a function of  $\omega$  for different sub-box lengths  $\ell$  (viz.  $\ell = 8, 10, 12$ ), we find the intersection point to be  $\omega_c = 0.0215(2)$  (in Fig. 6 (a)). This estimate reasonably agrees with the previously obtained value  $\omega_c = 0.0225(2)$  from the percolation study.  $B_\ell(\omega)$  follows a FSS relation similar to Eq. (7), which is then utilized to obtain the correlation exponent of the PS transition as  $\nu^M = 0.78(3)$  from the scaling collapse (see Fig. 6 (b))

For the order parameter  $\tilde{\phi}$ , the susceptibility can be defined as

$$\tilde{\chi} = \frac{1}{\ell^2} (\langle \Delta N_\ell^2 \rangle - \langle \Delta N_\ell \rangle^2). \quad (10)$$

Both  $\tilde{\phi}$  and  $\tilde{\chi}$  obey a FSS relation similar to Eq. (7); their scaling collapse (described respectively in Figs. 6 (c) and (d)), results in order parameter exponent  $\beta^M = 0.12(3)$  and susceptibility exponent  $\gamma^M = 1.32(8)$ . As listed in Table I, the critical exponents obtained from the percolation study of the RTPs at the critical point ( $\omega_c = 0.0225(2)$ ,  $J_c = 0.60(0)$ ), were  $\nu = 0.77(3)$ ,  $\beta = 0.041(3)$ , and  $\gamma = 1.458(60)$ . In comparison, the MIPS analysis of the same system yields the corresponding values as  $\nu^M = 0.78(3)$ ,  $\beta^M = 0.12(3)$ , and  $\gamma^M = 1.32(8)$ . Although

these two sets of exponents are different, a closer inspection reveals a deeper connection among them. Specifically, the correlation length exponents  $\nu$  and  $\nu^M$  are identical within error bounds, indicating that the length scales ( $\xi$ ) of the two phenomena are consistent with each other. For the order parameter exponent, while  $\beta$  and  $\beta^M$  are not numerically equal, they are related through the scaling relation described in Eq. (8). In fact, we observe that  $\beta^M = \frac{12}{5}\beta \approx 0.1$ , which matches with the scaling relation within the margin of error. Additionally, the susceptibility exponents  $\gamma$  and  $\gamma^M$  satisfy their respective hyperscaling relations ( $\gamma = d\nu - 2\beta$  in percolation and  $\gamma^M = d\nu^M - 2\beta^M$  in MIPS), further supporting the consistency between the two frameworks.

### C. The phase diagram

Building upon the insights gained from the critical exponent analysis, we now turn our attention to the global structure of the phase space governing the percolation transition. Understanding how the transition unfolds across the full range of system parameters provides a comprehensive picture that complements the local scaling behavior discussed in the previous section. The phase diagram shown in Fig. 3 presents a density plot of the order parameter  $\phi$  (defined in Eq. (3)) in the  $\omega$ - $J$  plane. Since the transition occurs within a narrow range of  $\omega$  (corresponding to high activity/motility), the  $\omega$ -axis is displayed on a logarithmic scale to enhance the visibility of the critical behavior. To further explore the limiting cases of our model, the phase diagram is replotted in Fig. 7. The horizontal dashed-dot line indicates  $J = J_c^* = 2\ln(1 + \sqrt{2})$ , the critical interaction strength for equilibrium phase separation in the corresponding CLG model. As  $\omega \rightarrow \infty$ , the system becomes passive, and accordingly, the critical line approaches this equilibrium limit:  $J_c \rightarrow J_c^*$ .

Several limiting cases offer deeper insights. When  $p = 1$ , particles move isotropically, with their internal orientation playing no role in the dynamics. In this case, the model reduces to the simple case of 2D CLG model, which undergoes phase separation at  $J_c^*$ . Thus, this horizontal line also represents the critical line of the IRTP model in the  $p = 1$  limit. In contrast, setting  $p = 0$  reduces our model to the one studied in Ref. [42], where PS transition occurs when  $J$  crosses a threshold  $J_c(\omega)$  which is larger than  $J_c^*$  for any finite  $\omega$ ; thus a stronger attractive interaction is required for the particles to phase separate. The PS transition observed in the absence of any translational diffusion ( $p = 0$ ) may be termed as *interaction-induced phase separation* (IIPS), as increased activity ( $\omega^{-1}$ ) here suppresses cluster formation and the system needs interaction to phase separate. This suppression is likely due to an effective repulsion induced by the active motion of attractive particles, as suggested in Ref. [46].

However, when translational diffusion is introduced

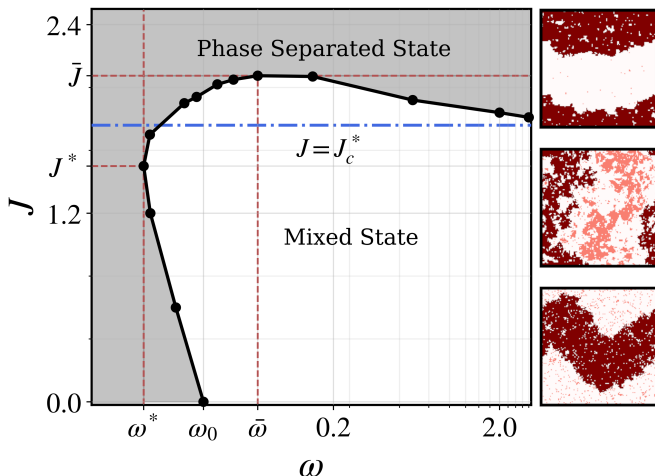


FIG. 7. (Color online) Phase diagram of the IRTP model in  $\omega$ - $J$  plane for  $\rho = 0.5$  and  $p = 0.05$ . The critical line is drawn by joining the estimated critical points (dots) from Table. I, separates the PS transition from the mixed one. Important features: (i) No transition occurs and the system remains in PS state, when  $J > \bar{J} = 2.075$  or when  $\omega < \omega^* = 0.0144$ ; note that  $J = \bar{J}$  and  $\omega = \omega^*$  (dashed lines) bound the critical line. (ii) For  $J = 0$  the system exhibits a MIPS transition at  $\omega = \omega_0 = 0.0330(2)$ . (iii) In the range  $\omega^* \leq \omega \leq \bar{\omega}$  the area of the PS state increases with the increase of motility  $\omega^{-1}$ ; phase transitions occurring in this regime may be termed as MIPS transition as motility helps the system to phase separate. (iv) For  $\omega > \bar{\omega} = 0.07$  (at  $\omega = \bar{\omega}$  the line  $J = \bar{J}$  is tangent to the critical line) the PS state region starts decreasing with increased motility and the transition here is rather interaction-induced. (v) In the regime  $\omega^* \leq \omega \leq \omega_0$ , MIPS transition is re-entrant – the MIPS phase existing at small  $J$  gets destroyed as  $J$  is increased and reappears again for higher  $J$ . The typical configurations of the system in this re-entrant region (at  $\omega = 0.015$ ) are shown beside the phase diagram for three different  $J = 0.0, 1.4, 2.8$  (bottom to top).

( $p > 0$ ), the nature of the critical line changes. For example, with  $p = 0.05$  MIPS transition occurs even at weak or zero attraction, as shown in Fig. 7. The shaded region in the figure represents the PS state, bounded by a critical line (solid line with circles). For the non-interacting case ( $J = 0$ ), now a MIPS transition occurs at  $\omega = \omega_0 = 0.0330$ , in line with the findings of Ref. [43], which demonstrated that MIPS can arise at finite tumble rates when  $p > 0$ .

The horizontal dashed line  $J = \bar{J}$  and the vertical dashed line  $\omega = \omega^*$  are tangent to the critical line at ( $\bar{\omega} = 0.07, \bar{J} = 2.075$ ) and ( $\omega^* = 0.0144, J^* = 1.5$ ) respectively, which means the IRTP system phase separates for any  $J > \bar{J}$  (irrespective of  $\omega$ ) and any  $\omega < \omega^*$  (irrespective of  $J$ ). In the regime  $\omega^* < \omega < \bar{\omega}$  – motility does enhance the stability of the PS state, as the region of PS state increases with increased motility. Due to this fact, the PS transition occurring here can be termed as motility-induced phase separation transition (MIPS), and on the other hand motility suppresses cluster forma-

tion when  $\omega > \bar{\omega}$ ; here the PS transition is interaction induced.

Another interesting feature that can be observed from the phase diagram is that we have a re-entrant phase transition in the regions: (a)  $\omega^* \leq \omega \leq \omega_0$  and (b)  $J^* \leq J \leq \bar{J}$ . In the first case, when one keeps increasing  $J$  while keeping  $\omega$  fixed, the system first enters from a PS state to a mixed one and transits again to the PS state with a further increase of  $J$ . The same happens in the second case when  $\omega$  is increased keeping  $J$  fixed.

We end this section with the following note. In this article, the PS transition of the IRTP model is studied at a specific value of  $p$ , which is 0.05. However, this choice is in no way special; we expect the qualitative features of the phase diagram to persist for any  $p > 0$ .

## V. ROLE OF DENSITY

So far we have studied the percolation and MIPS transition of RTPs at conserved particle density  $\rho = 1/2$ , expecting that the critical density is not very different from it; in fact,  $\rho = 1/2$  is indeed the exact critical density for the passive counterpart (2D CLG), which obey  $\tilde{\phi} \rightarrow -\tilde{\phi}$  (or particle-hole) symmetry. Due to the absence of such symmetry in the IRTP model, to estimate the critical point and the critical exponents, one needs to tune two parameters ( $\rho$  and  $\omega$ ) simultaneously for a fixed interaction strength  $J$ . For such a situation, a finite size scaling method was first proposed for Ising-like models in Ref. [52] and later put forward to liquid-gas phase transitions in Ref. [65]. The basic idea was to divide the system of size  $L$ , into square sub-boxes of size  $\ell = (L/n)^d$ , where  $n$  is an integer and  $d$  is the linear dimension. Now, even though the overall conserved density  $\rho$  is fixed, these sub-boxes possess their own fluctuating number of particles, leading to a steady state sub-system density distribution function  $P(\rho)$ .

This approximation of  $P(\rho)$  in [52, 65], however, suffers from interface overlap between two phases. In the subsequent improved work [41], an elongated simulation box of aspect ratio 3 : 1 was taken as described in Section III. With this setup, in the PS state the bulk liquid and gas phases can be accurately sampled through the four sub-boxes while avoiding considerable overlap with the in-between interface region comprising parts of the liquid and gas phases. In this elongated geometry, the edges of the bulk phases (each of an area  $\ell \times 2\ell$ ) are  $2\ell$  apart from one another, and each edge lies on an average  $\ell$  distance away from the interface. Due to the isotropic growth (as expected for systems belonging to IUC), the correlation length  $\xi$  is forced to grow up to a maximum of  $2\ell$ , which is the shorter length of the system. So in the region  $\omega < \omega_c$ , when  $\xi \ll 2\ell$ , the interfacial fluctuation would not distort the bulk phases and thus the samples collected from liquid (dense sub box) and gas (dilute sub box) become uncorrelated. Then  $P(\rho)$  constructed from the independent samples collected from all four sub-boxes

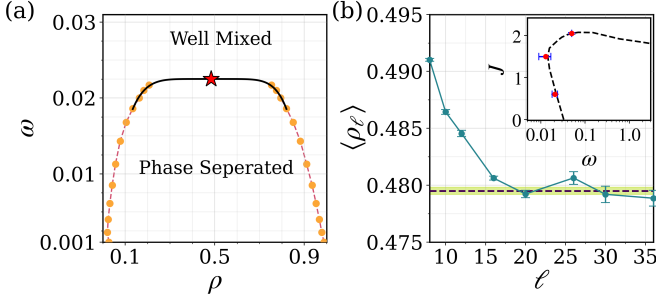


FIG. 8. (Color online) Coexistence line and critical density estimation: (a) Coexistence densities  $\rho_+$  and  $\rho_-$  are plotted for different  $\omega$  for  $J_c = 0.6$  case, along with estimated critical point denoted as star ( $\rho_c = 0.4795(3)$ ,  $\omega_c = 0.0225$ ). Points far from the critical point are connected through a dashed line as a guide to the eye and for the close ones, both the liquid and gas branches are fitted with a power law, where the exponent  $\beta^M = 0.15$  matches well within the error bounds with the one obtained from the FSS collapse of  $\phi$  (Eq. (2)). For all points, uncertainties are smaller than the respective point size. (b) Average density  $\langle\rho_\ell\rangle$  of sub-boxes is plotted with sub-box size  $\ell$  for  $J_c = 0.6$ . The dashed line is the estimate of  $\rho_c = 0.4795(3)$  and the shaded region is the error in it. In the inset, critical points obtained with newly estimated densities at  $J_c = 0.6$  and  $1.5$  and at  $\omega_c = 0.6$  are shown with their respective uncertainties. The dashed line is constructed with the critical points obtained with  $\rho_c = \frac{1}{2}$  from Table. (I).

would result in a double-peaked profile.

Contrary to this in the region  $\omega > \omega_c$ , density fluctuations are of the order of  $\xi$ , which itself is very small ( $\xi \ll 2\ell$ ), thereby making the density samples of the four boxes homogeneous. Corresponding  $P(\rho)$  is expected to be a Gaussian centered at the system's average density  $\langle\rho_\ell\rangle$ . Further, in the critical region when the correlation length  $\xi$  grows to an extent that is comparable to the sub-box size  $\ell$  ( $\xi \simeq \ell$ ), and due to that the distribution becomes non-gaussian, but follows a universal scaling function [65]

$$P(\rho) = \ell^{\beta^M/\nu^M} \mathcal{F}(\Delta \ell^{\beta^M/\nu^M}, \ell^{1/\nu^M} |\varepsilon|) \quad (11)$$

where  $\mathcal{F}(\cdot)$  is a scaling function,  $\Delta = (\rho - \rho_c)$  and  $\varepsilon = \omega - \omega_c$ . This universal scaling form asserts that choosing  $\rho = 1/2$  as the critical value does not compromise the accurate estimation of the other critical parameters and exponents. This assertion is well supported by the convergence of Binder cumulant ( $B_\ell$  or  $B_L$ ) for both the sub-box method and percolation study at a single point (see Fig. 4 (a) and Fig. 6 (a)), otherwise the density-dependent corrections in Eq. (11) would have prevented it.

Now for the determination of the actual critical density, we note that the average density  $\langle\rho_\ell\rangle$  of all the four sub-boxes measured at the critical point  $\omega_c$ , saturates to a critical value  $\rho_c$  as  $\ell \rightarrow \infty$ . For  $J_c = 0.6$ , we see from Fig. 8 (b) that the average density  $\langle\rho_\ell\rangle$  corresponding to different  $\ell$ , calculated by averaging density samples

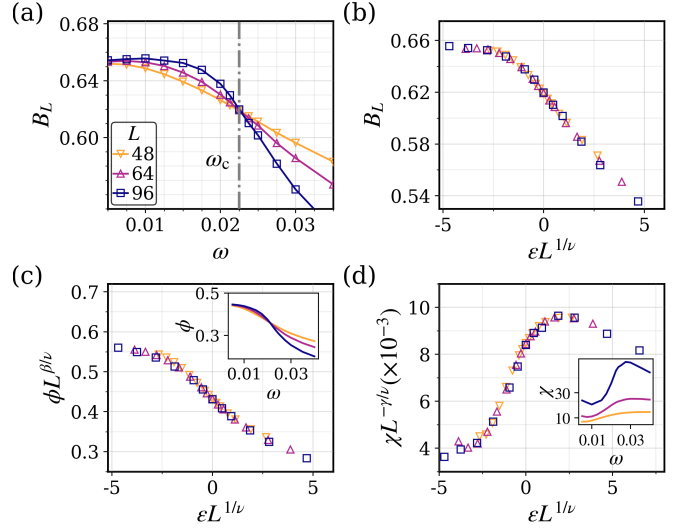


FIG. 9. (Color online) FSS collapse plot from percolation study for interaction strength  $J_c = 0.6$  at estimated critical density  $\rho_c = \langle\rho_\ell\rangle = 0.4795(3)$ . The critical point shown by the dashed line in (a) is the same as obtained in the case of density  $\rho_c = 0.5$  Fig. 4, which is  $\omega_c = 0.0225(2)$  for this case. Similarly from (b), (c) and (d) we estimated the critical exponents  $\nu$ ,  $\beta$ , and  $\gamma$  to be same as that of Fig. 4, as in this case they are:  $0.77(3)$ ,  $0.041(3)$  and  $1.458(60)$  respectively.

obtained from all independent runs and over all sub-box sizes, saturates to  $\rho_c = 0.4795(3)$ . This  $\rho_c$  is calculated by averaging density samples obtained from all independent runs and over all sub-box sizes for which  $\ell \geq 20$  at  $\omega_c$ . To ascertain that  $\omega_c$  and the critical exponents remain the same within the error limits, we again study the percolation transition of the IRTP model at  $J = 0.6$ , with particle density set at this newly estimated critical value  $\rho_c = 0.4795$ . From the crossing point of  $B_L$  vs  $\omega$  curves in Fig. 9 (a) we get  $\omega_c = 0.0225(2)$  which matches well with the  $\omega_c$  value listed in Table I for  $\rho = 1/2$ . Moreover,  $B_L$ ,  $\phi L^{\beta/\nu}$  and  $\chi L^{-\gamma/\nu}$  exhibit good data collapse when plotted against  $\varepsilon L^{1/\nu}$ , for  $\nu = 0.77(3)$ ,  $\beta = 0.041(3)$  and  $\gamma = 1.458(60)$  which agree well with the critical exponents listed in Table I within their respective margins of error.

These findings confirm that the estimated critical parameters at  $\rho_c = 0.4795(3)$  are consistent with those obtained at  $\rho_c = 0.5$ . The agreement across different system sizes and methods demonstrates that the finite-size scaling analysis remains valid even with this refined estimate and thereby matches well with the assertion given in [44].

#### A. The Coexistence line and the critical density

The density samples of the dense and dilute boxes  $\rho_\pm$ , calculated from Eq. (2) can be utilized to obtain the phase-coexistence line of the system. For  $J_c = 0.6$ , we have shown the plot of the co-existence line for different  $\omega$  values in Fig. 8 (a). As  $\omega$  approaches its critical value

$\omega_c = 0.0215(2)$ , both  $\rho_+$  and  $\rho_-$  are expected to reach a unique value  $\rho_c$  but the correlation length  $\xi$  of the system also becomes larger at the critical point. For that reason, the high and low-density regions are not well separated anymore due to substantial overlap from the interface region at the boundaries and it becomes increasingly difficult to distinguish  $\rho_+$  from  $\rho_-$ . We try to find the best-fit line that connects passes through  $\rho_{\pm}$  points determined for  $\omega < \omega_c$ . The curvature of the best-fit line (represented by a solid black line) near its maxima at  $\rho_c = 0.4795$ , determined in the previous section, is quite small as expected. Indeed  $\rho_c$  is not much different from  $\rho = 0.5$ ; also the critical exponents calculated at  $\rho_c = 0.4795$  do not differ appreciably from the same obtained at  $\rho = 0.5$ .

The co-existence lines for different  $J$  values are shown together in Fig. 1 in the 3D phase space  $J$ - $\rho$ - $\omega$ , with the critical points marked as stars. An interpolated surface passing through these coexistence lines separates the PS state (below this surface) from the well-mixed (above the surface) state. The critical line, obtained by joining these critical points (stars) is also shown in the 3D phase space. Initially, the area of the PS state decreases with increasing  $J$ , which is counter-intuitive, as the MIPS state existing for  $J = 0$  (the case of non-interacting RTPs) is destroyed as one introduces attraction among the particles. These results are, however consistent with earlier works [22, 23] of a system of RTPs with attractive interaction. It is also consistent with the exact results of [46] obtained for two active particles, where authors show that attractive interaction generates effective repulsion among the particles, and works against large cluster formation. For very large  $J$ , the effect of activity is insignificant and at that limit, phase separation occurs rather due to attractive interaction, not due to motility; hence it can be concluded that PS transition for large  $J$  is only interaction-induced, similar to what one sees in equilibrium lattice gas models.

## VI. SUPER-UNIVERSALITY OF PERCOLATION AND MIPS TRANSITIONS

Throughout this study we observe that critical exponents of percolation and hence the corresponding exponents of MIPS transition vary continuously, maintaining the hyperscaling relations  $2\beta + \gamma = d\nu$ , within error limits. The variation of exponents for this IRTP model is shown in Fig. 10. These continuously varying critical exponents suggest the existence of a marginal operator in the system (identifying such a marginal operator is beyond the scope of this work though). Recently it was proposed that systems with continuously varying critical exponents form a super universality class in the sense that certain scaling functions remain invariant all along the critical line; these scaling functions are identical to that of the parent universality class [33, 66]. One such scaling function is the Binder cumulant  $B_L$  expressed as

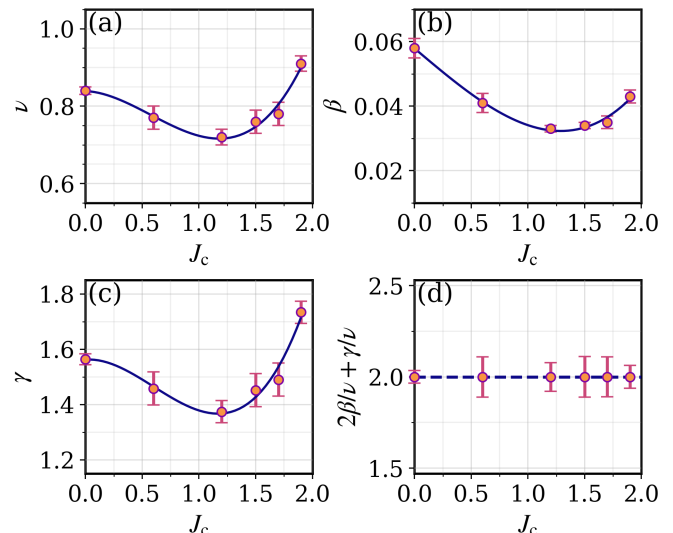


FIG. 10. (Color online) Continuous variation of the percolation exponents: (a)  $\nu$ , (b)  $\beta$  and (c)  $\gamma$  of IRTP model along the critical line shown as a function of  $J_c$  (taken from Table I). The solid lines are cubic fit to the existing data. (d) shows that the exponents obey the hyperscaling relation  $d = 2\beta/\nu + \gamma/\nu$ .

a function of a variable  $\xi_2/L$ , where  $\xi_2$  represents the second moment of the correlation length  $\xi$ , defined as follows

$$(\xi_2)^2 = \frac{\int_0^\infty r^2 C(\mathbf{r}) d\mathbf{r}}{\int_0^\infty C(\mathbf{r}) d\mathbf{r}}; \quad C(\mathbf{r}) = \langle n_i n_{i+\mathbf{r}} \rangle - \rho^2$$

As, Binder cumulants are already calculated along the neighborhood of the critical line to estimate the critical thresholds ( $\omega_c, J_c$ ), it only remains for us to calculate  $\xi_2$  from the pair correlation function  $C(r)$  (where  $r = |\mathbf{r}|$ ), obtained through MC simulations near the critical line. In Fig. 11, a plot of the Binder cumulants  $B_L$  corresponding to different interaction strengths against the quantity  $\xi_2/L$  is shown as a parametric function of different critical points ( $\omega_c, J_c$ ) for different  $L$  values. It is evident from the figure that these curves match quite well with each other irrespective of the value of the critical threshold and the system size; more importantly, independent of the value of the critical exponents which vary continuously along the line. Along with these super-universal curves, we have also plotted the corresponding scaling function of  $Z_2P$ , obtained here for correlated site percolation in 2D CLG model at criticality (shown by the dashed line in Fig. 11). A very good alignment among the scaling functions of the IRTP model with that of the CLG model provides clear evidence that the geometric transition of RTPs in 2D forms a  $Z_2P$  super universality class.

Further, since the critical exponents  $\nu^M, \beta^M, \gamma^M$  of the underlying MIPS transition are only scaled variants of the percolation critical exponents and follow Eq. (5), they also vary continuously along the critical line in a

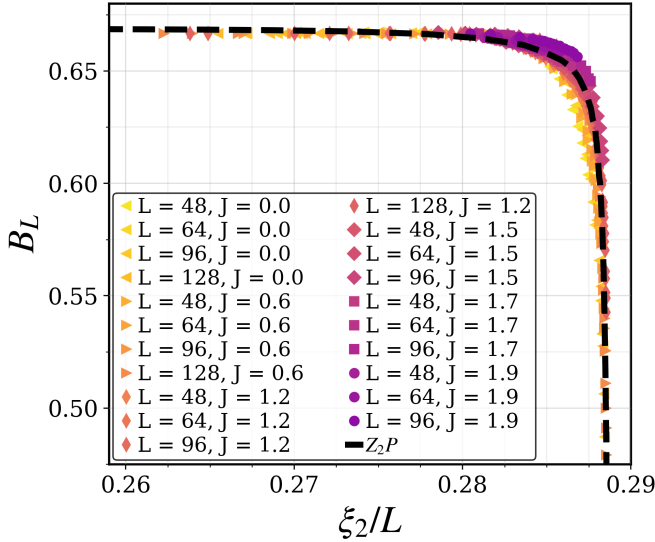


FIG. 11. (Color online) Plot of  $B_L$  vs  $\xi_2/L$  as a function of  $\omega$  for different values of  $J$  and  $L$ . The dashed solid line represents the same scaling function of  $Z_2P$  universality class, obtained by simulating 2D lattice gas model.

similar fashion. Consequently, we conclude that the PS transition in IRTP model belongs to  $Z_2$  super universality class (or Ising super universality class) [33, 66].

## VII. CONCLUSION AND DISCUSSION

In our IRTP model, although we choose the Metropolis rate following the energy function (Eq. (1)) identical to the equilibrium CLG models, the system does not obey detailed balance due to the directional asymmetry in their motion for any  $0 \leq p < 1$ . This asymmetry forces the system to be in a nonequilibrium steady state and the phase separation for any  $p < 1$  occurs as a nonequilibrium phase transition. Also, depending on all the parameters of the model: the conserved particle density  $\rho$ , tumbling rate  $\omega$  (or motility  $\omega^{-1}$ ), translational diffusion  $p$  and attractive interaction strength  $J$ , our extensive numerical simulations results in the following conclusions.

- In the absence of any translational diffusion ( $p = 0$ ), motility hinders cluster formation, as larger attractive interaction is required with increased motility, i.e.  $J_c(\omega) < J_c(\infty)$ ;  $\forall \omega > 0$ . A representative figure is shown in Fig. 12 (a). In this case, we only have an interaction-induced phase separation transition (IIPS).
- For  $J = 0$ , we observed a PS transition in  $\omega$ - $p$  which is purely motility induced. Since the system is well mixed for all  $\omega$  when  $p = 0$  (as discussed above) and  $p = 1$  (the model reduces to the symmetric exclusion process (SEP) where all configurations are equally likely), the MIPS transition must be re-entrant: for small  $\omega > 0$  the system starts with a

mixed phase at  $p = 0$  and enters a phase separated state (PS state) as  $p$  is increased, further increase of  $p$  destroy the PS state leading to another phase transition (PS state to mixed state). Fig. 12 (b) demonstrates this  $J = 0$  situation.

- When  $p \neq 0$  but fixed, there is an MIPS transition at  $J = 0$ , where RTPs phase separate when  $\omega$  decreases below a threshold  $\omega_c > 0$ . Although there is no explicit interaction provided externally, particles generate an effective non-reciprocal interaction because of their high motility (low  $\omega$ ), which is responsible for the transition. We find that any additional attraction  $J > 0$  acts against cluster formation: the PS state existing at  $J = 0$  is destroyed when  $J$  is increased keeping  $\omega$  fixed - a further increase of  $J$  results in a PS transition again, this time it is interaction-induced however. The phase diagram is described in Fig. 12 (c) for  $p = 0.05$ .

In all these studies, density was kept fixed at  $\rho = 1/2$ , which is indeed the critical density of the passive particles (2D CLG), phase separating in the absence of directional asymmetry ( $p = 0$ ). But in the PS state of active RTPs, the system maintains two different densities:  $\rho_+$ , and  $\rho_-$ , which keep changing along the co-existence line as the model parameters ( $T$  or  $\omega$ ) vary, eventually reaching a critical point where they become equal,  $\rho_{\pm} = \rho_c$ , creating a homogeneous density profile throughout the system. Since  $\rho_{\pm}$  forms different branches, at their meeting point, one expects them to have a vanishing slope at  $\rho_c$ . Indeed,  $\rho_c$  is different from  $\rho = 1/2$ , but the deviation is not significant for the cases we have calculated explicitly. We also showed that our estimated critical exponents are robust and do not depend on the actual value of  $\rho_c$  as long as it is close to  $1/2$ . One of the reasons for this insensitivity is possibly the low curvature of the coexistence line near its maximum. A complete phase diagram of the model in the  $J$ - $\omega$ - $\rho$  phase space is shown in Fig. 1 for  $p = 0.05$ , where a dome-like coexistence surface separates the PS state from the mixed (homogeneous) phase, and the maximal points on the surface form a critical line.

We also investigate the nature of criticality along the critical line to determine the universality class of the PS transition in IRTP model. It turns out that the critical exponents vary continuously along the critical line, similar to equilibrium critical behavior along a marginal direction. Recent studies propose that systems with continuously varying critical exponents form a “super universality class” [33, 66] when some of their scaling functions match those obtained for a parent universality class. Since in the  $\omega \rightarrow \infty$  limit particles become passive resulting in an equilibrium PS transition at  $J_c^* = 2 \ln(1 + \sqrt{2})$ ,  $\rho_c = 1/2$ , belonging to the Ising universality class (IUC), we anticipate that the parent universality class of PS transition must be the IUC. Indeed we find that, all along the critical line, the scaling function,  $B_L$  of the geometric transition as a function of  $\xi_2/L$ , matches well with the same obtained for the per-

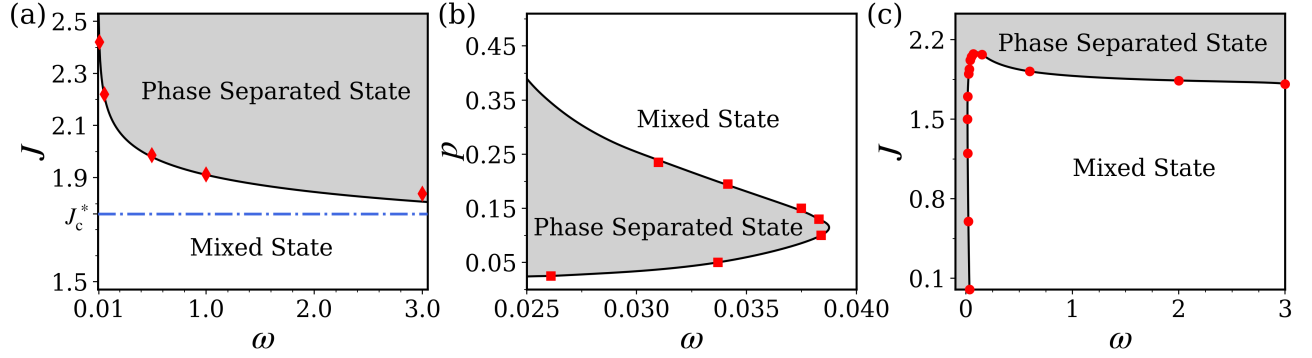


FIG. 12. (Color online) Phase diagram of IRTP model for  $\rho = 0.5$  in (a)  $\omega$ - $J$  plane (for  $p = 0$ ), (b)  $\omega$ - $p$  plane (for  $J = 0$ ), and (c)  $\omega$ - $J$  plane (for  $p = 0.05$ ). In all three cases, estimated critical points (symbols) are joined by best-fit lines (the critical line) that separate the PS state from the mixed ones.

colation transition of the lattice gas model belonging to  $Z_2P$  universality class. This implies that the PS transition in IRTP model falls in the  $Z_2$  super universality class.

In conclusion, we have studied a system of interacting run-and-tumble particles (IRTPs) on a square lattice that interact via nearest-neighbor attraction and obey steric constraints, forbidding multiple occupancy. This minimal model captures rich phase behavior, exhibiting phase separation transitions driven by motility, interaction, or a combination of both. We find that the critical behavior of the motility-induced phase separation (MIPS) transition belongs to the Ising super universality class. Importantly, lattice-based models like this provide a significant advantage: in certain limits, they reduce to exactly solvable equilibrium models. This connection anchors the critical behavior of active systems to well-established results in equilibrium statistical mechanics, allowing for analytical insight beyond numerical estimates. Our analysis also reveals some counterintuitive effects of motility. In the absence of translational diffusion, motility can suppress cluster formation, whereas in its presence, it induces an effective attraction that facilitates phase separation. Sur-

prisingly, when combined with explicit attractive interactions, the overall effective attraction appears to weaken. To understand these phenomena more deeply, we are extending our study to systems with a small number of particles, where exact steady states may be accessible and illuminating.

#### ACKNOWLEDGMENT

We acknowledge the Kepler Computing Facility, maintained by the Department of Physical Sciences at IISER Kolkata, for providing the computational support necessary for this study. SM gratefully acknowledges financial support through a National Postdoctoral Fellowship from the Anusandhan National Research Foundation (ANRF), Department of Science and Technology, Government of India, under project File no: PDF/2023/002952. PKM acknowledges the support provided by ANRF, Science and Engineering Research Board (SERB), Department of Science and Technology, Govt. of India under Grant No. MTR/2023/000644.

- 
- [1] M. C. Marchetti, J. F. Joanny, S. Ramaswamy, T. B. Liverpool, J. Prost, M. Rao, and R. A. Simha, Hydrodynamics of soft active matter, *Rev. Mod. Phys.* **85**, 1143–1189 (2013).
  - [2] M. Ballerini, N. Cabibbo, R. Candelier, A. Cavagna, E. Cisbani, I. Giardina, V. Lecomte, A. Orlandi, G. Parisi, A. Procaccini, M. Viale, and V. Zdravkovic, Interaction ruling animal collective behavior depends on topological rather than metric distance: Evidence from a field study, *PNAS* **105**, 1232–1237 (2008).
  - [3] Y. Katz, K. Tunström, C. C. Ioannou, C. Huepe, and I. D. Couzin, Inferring the structure and dynamics of interactions in schooling fish, *PNAS* **108**, 18720–18725 (2011).
  - [4] V. Schaller, C. Weber, C. Semmrich, E. Frey, and A. R. Bausch, Polar patterns of driven filaments, *Nat. Commun.* **467**, 73–77 (2010).
  - [5] Y. Sumino, K. H. Nagai, Y. Shitaka, D. Tanaka, K. Yoshikawa, H. Chaté, and K. Oiwa, Large-scale vortex lattice emerging from collectively moving microtubules, *Nat. Commun.* **483**, 448–452 (2012).
  - [6] I. Theurkauff, C. Cottin-Bizonne, J. Palacci, C. Ybert, and L. Bocquet, Dynamic clustering in active colloidal suspensions with chemical signaling, *Phys. Rev. Lett.* **108** (2012).
  - [7] I. Buttinoni, J. Bialké, F. Kümmel, H. Löwen, C. Bechinger, and T. Speck, Dynamical clustering and phase separation in suspensions of self-propelled colloidal particles, *Phys. Rev. Lett.* **110** (2013).
  - [8] J. Palacci, S. Sacanna, A. P. Steinberg, D. J. Pine, and P. M. Chaikin, Living crystals of light-activated colloidal surfers, *Science* **339**, 936–940 (2013).

- [9] A. Bricard, J.-B. Caussin, N. Desreumaux, O. Dauchot, and D. Bartolo, Emergence of macroscopic directed motion in populations of motile colloids, *Nat. Commun.* **503**, 95–98 (2013).
- [10] M. J. Schnitzer, Theory of continuum random walks and application to chemotaxis, *Phys. Rev. E* **48**, 2553–2568 (1993).
- [11] H. C. Berg, *E. coli in Motion* (Springer New York, 2004).
- [12] P. Romanczuk, M. Bär, W. Ebeling, B. Lindner, and L. Schimansky-Geier, Active brownian particles: From individual to collective stochastic dynamics, *Eur. Phys. J. Spec. Top.* **202**, 1–162 (2012).
- [13] M. Polin, I. Tuval, K. Drescher, J. P. Gollub, and R. E. Goldstein, Chlamydomonas swims with two “gears” in a eukaryotic version of run-and-tumble locomotion, *Science* **325**, 487–490 (2009).
- [14] M. E. Cates and J. Tailleur, When are active brownian particles and run-and-tumble particles equivalent? consequences for motility-induced phase separation, *Europhys. Lett.* **101**, 20010 (2013).
- [15] J. Tailleur and M. E. Cates, Sedimentation, trapping, and rectification of dilute bacteria, *Europhys. Lett.* **86**, 60002 (2009).
- [16] M. Enculescu and H. Stark, Active colloidal suspensions exhibit polar order under gravity, *Phys. Rev. Lett.* **107**, 10.1103/physrevlett.107.058301 (2011).
- [17] C. F. Lee, Active particles under confinement: aggregation at the wall and gradient formation inside a channel, *New J. Phys.* **15**, 055007 (2013).
- [18] A. Slowman, M. Evans, and R. Blythe, Jamming and attraction of interacting run-and-tumble random walkers, *Phys. Rev. Lett.* **116** (2016).
- [19] A. B. Slowman, M. R. Evans, and R. A. Blythe, Exact solution of two interacting run-and-tumble random walkers with finite tumble duration, *J. Phys. A: Math. Theor.* **50**, 375601 (2017).
- [20] C. O. Reichhardt and C. Reichhardt, Ratchet effects in active matter systems, *Annu. Rev. Condens. Matter Phys.* **8**, 51–75 (2017).
- [21] M. E. Cates and J. Tailleur, Motility-induced phase separation, *Annu. Rev. Condens. Matter Phys.* **6**, 219–244 (2015).
- [22] G. S. Redner, M. F. Hagan, and A. Baskaran, Structure and dynamics of a phase-separating active colloidal fluid, *Phys. Rev. Lett.* **110** (2013).
- [23] G. S. Redner, A. Baskaran, and M. F. Hagan, Reentrant phase behavior in active colloids with attraction, *Phys. Rev. E* **88**, 012305 (2013).
- [24] J. Stenhammar, A. Tiribocchi, R. J. Allen, D. Marenduzzo, and M. E. Cates, Continuum theory of phase separation kinetics for active brownian particles, *Phys. Rev. Lett.* **111** (2013).
- [25] A. Patch, D. Yllanes, and M. C. Marchetti, Kinetics of motility-induced phase separation and swim pressure, *Phys. Rev. E* **95** (2017).
- [26] Y. Fily and M. C. Marchetti, Athermal phase separation of self-propelled particles with no alignment, *Phys. Rev. Lett.* **108** (2012).
- [27] J. Bialké, H. Löwen, and T. Speck, Microscopic theory for the phase separation of self-propelled repulsive disks, *Europhys. Lett.* **103**, 30008 (2013).
- [28] F. Schweitzer, An agent-based framework of active matter with applications in biological and social systems, *Eur. J. Phys.* **40**, 014003 (2018).
- [29] A. Ziepke, I. Maryshev, I. S. Aranson, and E. Frey, Multi-scale organization in communicating active matter, *Nat. Commun.* **13** (2022).
- [30] A. G. Thompson, J. Tailleur, M. E. Cates, and R. A. Blythe, Lattice models of nonequilibrium bacterial dynamics, *J. Stat. Mech.: Theory Exp.* **2011** (02), P02029.
- [31] E. Mallmin, R. A. Blythe, and M. R. Evans, Exact spectral solution of two interacting run-and-tumble particles on a ring lattice, *J. Stat. Mech.: Theory Exp.* **2019** (1), 013204.
- [32] R. Dandekar, S. Chakraborti, and R. Rajesh, Hard core run and tumble particles on a one-dimensional lattice, *Phys. Rev. E* **102** (2020).
- [33] I. Mukherjee and P. K. Mohanty, Hidden superuniversality in systems with continuous variation of critical exponents, *Physical Review B* **108** (2023).
- [34] M. Kourbane-Houssene, C. Erignoux, T. Bodineau, and J. Tailleur, Exact hydrodynamic description of active lattice gases, *Phys. Rev. Lett.* **120** (2018).
- [35] F. Dittrich, T. Speck, and P. Virnau, Critical behavior in active lattice models of motility-induced phase separation, *Eur. Phys. J. E* **44** (2021).
- [36] S. Whitelam, K. Klymko, and D. Mandal, Phase separation and large deviations of lattice active matter, *J. Chem. Phys.* **148** (2018).
- [37] L. Yao and R. L. Jack, Interfacial and density fluctuations in a lattice model of motility-induced phase separation, *J. Chem. Phys.* **162** (2025).
- [38] R. Soto and R. Golestanian, Run-and-tumble dynamics in a crowded environment: Persistent exclusion process for swimmers, *Phys. Rev. E* **89** (2014).
- [39] A. P. Solon, J.-B. Caussin, D. Bartolo, H. Chaté, and J. Tailleur, Pattern formation in flocking models: A hydrodynamic description, *Phys. Rev. E* **92** (2015).
- [40] N. Sepúlveda and R. Soto, Coarsening and clustering in run-and-tumble dynamics with short-range exclusion, *Phys. Rev. E* **94**, 10.1103/physreve.94.022603 (2016).
- [41] J. T. Siebert, F. Dittrich, F. Schmid, K. Binder, T. Speck, and P. Virnau, Critical behavior of active brownian particles, *Phys. Rev. E* **98** (2018).
- [42] C. G. Ray, I. Mukherjee, and P. K. Mohanty, How motility affects ising transitions, *J. Stat. Mech.: Theory Exp.* **2024** (9), 093207.
- [43] S. K. Saha, A. Banerjee, and P. K. Mohanty, Site-percolation transition of run-and-tumble particles, *Soft Matter* **20**, 9503 (2024).
- [44] B. Partridge and C. F. Lee, Critical motility-induced phase separation belongs to the ising universality class, *Phys. Rev. Lett.* **123** (2019).
- [45] C. Maggi, M. Paoluzzi, A. Crisanti, E. Zaccarelli, and N. Gnan, Universality class of the motility-induced critical point in large scale off-lattice simulations of active particles, *J. Soft Matter* **17**, 3807–3812 (2021).
- [46] R. Sarkar and U. Basu, Emergent short-range repulsion for attractively coupled active particles, *Soft Matter* **21**, 3595 (2025).
- [47] G. Gonnella, D. Marenduzzo, A. Suma, and A. Tiribocchi, Motility-induced phase separation and coarsening in active matter, *Comptes Rendus. Physique* **16**, 316–331 (2015).
- [48] J. Martin-Roca, R. Martinez, L. C. Alexander, A. L. Diez, D. G. A. L. Aarts, F. Alarcon, J. Ramirez, and C. Valeriani, Characterization of mips in a suspension of repulsive active brownian particles through dynamical

- features, *J. Chem. Phys.* **154**, 174901 (2021).
- [49] J. Tailleur and M. E. Cates, Statistical mechanics of interacting run-and-tumble bacteria, *Phys. Rev. Lett.* **100** (2008).
  - [50] L. Onsager, Crystal statistics. i. a two-dimensional model with an order-disorder transition, *Phys. Rev.* **65**, 117–149 (1944).
  - [51] M. Rovere, P. Nielaba, and K. Binder, Simulation studies of gas-liquid transitions in two dimensions via a subsystem-block-density distribution analysis, *Z. Phys. B* **90**, 215–228 (1993).
  - [52] K. Binder, Finite size scaling analysis of ising model block distribution functions, *Z. Phys. B* **43**, 119–140 (1981).
  - [53] L. Bai and D. Breen, Calculating center of mass in an unbounded 2d environment, *J. Graph. Tools* **13**, 53 (2008).
  - [54] D. Stauffer, Scaling theory of percolation clusters, *Phys. Rep.* **54**, 1–74 (1979).
  - [55] J. W. Essam, Percolation theory, *Rep. Prog. Phys.* **43**, 833–912 (1980).
  - [56] W. Janke and A. M. J. Schakel, Fractal structure of spin clusters and domain walls in the two-dimensional ising model, *Physical Review E* **71** (2005).
  - [57] S. Mitra, D. Saha, and A. Sensharma, Percolation in a distorted square lattice, *Phys. Rev. E* **99**, 012117 (2019).
  - [58] A. Coniglio and W. Klein, Clusters and ising critical droplets: a renormalisation group approach, *J. Phys. A: Math. Gen.* **13**, 2775 (1980).
  - [59] A. Coniglio, Percolation and critical points, *J. Phys.: Condens. Matter* **13**, 9039 (2001).
  - [60] S. Fortunato, Site percolation and phase transitions in two dimensions, *Phys. Rev. B* **66**, 054107 (2002).
  - [61] A. Banerjee, P. Jana, and P. K. Mohanty, Geometric percolation of spins and spin dipoles in the ashkin-teller model, *Phys. Rev. B* **111**, 014403 (2025).
  - [62] A. L. Stella and C. Vanderzande, Scaling and fractal dimension of ising clusters at the  $d=2$  critical point, *Phys. Rev. Lett.* **62**, 1067–1070 (1989).
  - [63] D. Stauffer and A. Aharony, *Introduction to Percolation Theory*, 2nd ed. (Taylor & Francis, London, 1994).
  - [64] See Supplemental Material for details of the dynamics, simulation and estimation of critical points and exponents of percolation and phase separation transition, in support of our claims.
  - [65] M. Rovere, D. W. Heermann, and K. Binder, The gas-liquid transition of the two-dimensional lennard-jones fluid, *J. Phys.: Condens. Matter* **2**, 7009–7032 (1990).
  - [66] A. Pelissetto and E. Vicari, Critical phenomena and renormalization-group theory, *Phys. Rev. B* **62**, 6393 (2000).